Waterborne Hyperbranched Polyurethane/Carbon Dot Decorated Hydroxyapatite Nanocomposite

Highlight

Current chapter describes synthesis of carbon dot decorated hydroxyapatite nanohybrid by a simple one pot hydrothermal process. Bio-based and waste materials were used in the synthesis of the nanohybrid. The aqueous extract of corm of *Colocasia esculenta* was used as the carbon dot precursor, whereas egg shell was used to obtain calcium oxide, which served as one of the precursors for hydroxyapatite. The synthesized nanohybrid was characterized by using different analytical and spectroscopic techniques, *viz.* FTIR, XRD, TEM, SEM/EDX and Raman spectroscopy. TEM study confirmed the formation of needle shaped hydroxyapatite (length 60-80 nm, average diameter 20-30 nm) with decorated carbon dot over its surface. Elemental analysis showed a Ca/P ratio of 1.69, which is close to the Ca/P ratio (1.67) found in natural bone. Biological assessment of the nanohybrid demonstrated excellent cytocompatibility, cell proliferation and alkaline phosphatase activity with MG63 osteoblast cell line. Carbon dot decorated hydroxyapatite nanohybrid was used to fabricate tannic acid based waterborne hyperbranched polyurethane by using an *in situ* polymerization technique. Substantial improvement in the mechanical and thermal properties of the nanocomposite was perceived. Fabricated nanocomposite was tested for osteogenic activities and the results confirmed its suitability as bone regenerating material. The overall results endorse the development of a sustainable polymeric nanocomposite with high load bearing ability and profound bioactivity, which can be employed for bone tissue engineering application.

Parts of this chapter are published in

Gogoi, S., Kumar, M., Mandal, B.B., & Karak, N. A renewable resource based carbon dot decorated hydroxyapatite nanohybrid and its fabrication with waterborne hyperbranched polyurethane for bone tissue engineering, *RSC Adv.* **6**, 26066--26076, 2016.

6.1. Introduction

Bone defects due to trauma, infections, tumors or congenital disorder have become genuine problem across the globe.[1] Hence, development of novel polymeric materials with unique biological properties is desirable for their application in bone regeneration process.[2,3] In this context, Chapter 5 made an effort to utilize bio-functionalized nanomaterial to fabricate waterborne hyperbranched polyurethane system as a non-invasive vehicle for bone tissue engineering. The idea behind such approach was to impart high target specific bioactivity to a synthetic material. In this context, the present chapter made an effort to adopt an alternative technique, i.e. to use nanomaterial with inherent osteogenic activity in the fabrication of biocompatible polymeric materials. Use of such biologically active nanomaterial eliminates the need of bio-functionalization for target specific biological application. Further, such approach may allow to use harsh polymerization condition, which could not be used in a bio-nano-functionalization process in order to preserve bio-activity of the biomolecule. This can provide further edge to design prosthetic material with tunable material characteristics.

In this regard, we have found nano hydroxyapatite (HAp) as the most promising material. HAp is the major constituent of natural bone.[4,5] It exhibits the ability to endorse integration of bone tissues with profound biocompatibility and osteoconductivity. Similarity in chemical composition, size, morphology and crystallinity with natural bone materials leads to the osteoblastic behavior of HAp.[6,7] In recent time, nanotechnology based approach has also been adopted to improve the properties of HAp by preparing nanohybrid systems with other nanomaterials. Main objective of such nanohybrids is to obtain composite materials with enhanced mechanical and biological properties. In this milieu, carbon based nanomaterials have gained substantial attraction. The state of literature revealed preparation of HAp/carbon nano tube (CNT) and HAp/graphene oxide (GO) nanohybrids with excellent osteoblast seeding activity.[8-12] These multifunctional combined systems exhibit superior properties than single phase HAp. In this regard, we found carbon dot (CD) as a fascinating nanomaterial to prepare hybrid system of HAp. It possesses graphitic carbon structure with various oxygen functional groups. CD was also found as a suitable nanomaterial for bone tissue engineering application as discussed in

Chapter 4 and 5. Therefore, it is expected that combination of HAp with CD can lead to a multifunctional system, which may be effectively used to fabricate polymeric prostheses with excellent biological activity and high mechanical performance.

Thus, the authors herein present a simple and sustainable one pot synthesis of CD decorated HAp nanohybrid (CD@HAp) for the first time. Considering the importance of utilization of renewable raw materials in place of conventional feed-stock, effort was made to use corms of *Colocasia esculenta* and commonly available bio-waste egg shell in the synthesis of the nanohybrid system. The aqueous extract of *C. esculenta* served simultaneously as CD precursor as well as the template to grow the HAp nanocrystals. The *in vitro* biocompatibility, cell proliferation and alkaline phosphatase (ALP) activity of this nanohybrid with MG63 human osteoblast cell line were investigated. This nanohybrid was *in situ* fabricated with tannic acid based waterborne hyperbranched polyurethane (WHPU) in order to develop a novel polymeric bone implant material with high load bearing ability. The *in vitro* biocompatibility and cell proliferation of the nanocomposite films with MG63 human osteoblast cell line were investigated. Further, as ALP activity indicates good osteoconductive behavior, hence the same was delved into in order to judge the suitability of the nanocomposite system for bone tissue engineering application.

6.2. Experimental

6.2.1. Materials

IPDI, PEG 600 and BD of similar grade and specifications were used as described in Sub-Chapter 2A (Section 2A.2.1.). Other chemicals used in the fabrication of WHPU/CD@HAp nanocomposite were BMPA, TA, TEA and THF. All these chemicals possessed similar grade and specifications as described in Sub-Chapter 2B (Section 2B.2.1.). Similarly, same HE and PAA as mentioned in Chapter 3 (Section 3.2.1.) were used in the modification of the nanocomposite. Corms of *C. esculenta* and egg shell (hen) used in the synthesis of the nanohybrid were collected locally from Tezpur University Market Complex, Assam, India. Orthophosphoric acid (H_3PO_4) was procured from Merck, India and used as received.

On the other hand, for biological test same MG63 human osteosarcoma cell line was used as mentioned in Chapter 4 (Section 4.2.1.). The cell culture was

maintained by using MEM supplemented with 10% (v/v) FBS and penicillin streptomycin (1x) according to the method described in Chapter 4 (Section 4.2.1. and 4.2.3.6.). Other bio-chemicals like Alamar Blue, PBS (pH 7.4), Live/Dead assay kit, calcein-AM, ethidium homodimer, β-glycerol phosphate disodium salt pentahydrate, L-ascorbic acid, trypsin-EDTA and dexamethasone used in the biological evaluation of the nanocomposite films were of same grade and specifications as mentioned in Chapter 4 (Section 4.2.1.).

6.2.2. Characterization

FTIR spectra of the nanohybrid and nanocomposite were recorded under same condition using the same spectrometer as stated in Sub-Chapter 2A (Section 2A.2.2.). Same photo-spectrometer was used to obtain UV-visible spectra of CD@HAp, CD and HAp as described in Sub-Chapter 2B (Section 2B.2.2.). The shape, size and decoration of CD@HAp, as well as its distribution over the polymer matrix were visually studied by HRTEM analysis using the same instrument and grid as mentioned in Chapter 4 (Section 4.2.2.). The microscopic data were analyzed for IFFT images by using Gatan Microscopy Suite Software as mentioned in the same chapter. Same instruments and experimental conditions were deployed for other characterizations of the nanohybrid and polymeric nanocomposite, which include EDX for elemental composition, XRD for diffraction patterns and Raman spectroscopy for the study of graphitic structure as described in Chapter 4 (Section 4.2.2.). Likewise, for the evaluation of thermal and mechanical properties, the same instruments and instrumentation techniques, such as TGA, DSC, UTM, scratch hardness tester, gloss meter, impact tester etc. were used as described in Sub-Chapter 2A (Section 2A.2.2.). Same fluorescence microscope in Live/Dead assay and multimode reader in Alamar Blue assay were used as mentioned in Chapter 4 (Section 4.2.2.).

6.2.3. Methods

6.2.3.1. Synthesis of CD@HAp

Egg shell was treated with dilute HNO_3 to remove the thin inner protein layer. Then, it was washed with water, dried inside an oven at 60 °C and crushed into powder with a pastel mortar. The crushed egg shell was calcinated at 900 °C for 4 h.[13] Calcium oxide (CaO) thus obtained was used as Ca source in the synthesis of the nanohybrid. An

aqueous dispersion of CaO was prepared. Calculated amount of H_3PO_4 was added drop wise (keeping Ca/P ratio 1.67) to the CaO dispersion under vigorous stirring by maintaining a basic condition (pH>10) using ammonium hydroxide. Then aqueous extract of corms of *C. esculenta* was added and mixed well by stirring for half an hour. The mixture was poured into a 200 mL Teflon lined autoclave, which was heated at 170 °C for 15 h. The dark brown colored liquor thus obtained was filtered through poly(tetrafluoro ethylene) filter paper. Residue was washed several times with distilled water to remove the unreacted reagents and un-adhered CD. Finally, the product was dried at 60 °C in an oven for 24 h and stored in a desiccator.

6.2.3.2. Fabrication of WHPU/CD@HAp nanocomposite

Required amount of IPDI, PEG 600 and BMPA were reacted (by maintaining -NCO/-OH ratio 1.5) in a four neck glass reactor equipped with a condenser, a nitrogen gas inlet and a mechanical stirrer. The reaction was carried out at 80±2 °C for 1.5 h. After the initial step, TA and BD were added using THF as the solvent and keeping -NCO/-OH ratio 1.1. The reaction was continued for 3.5 h at 70±2 °C. It was followed by the addition of CD@HAp and BD by adjusting -NCO/-OH ratio 1.0. The reaction was further carried out at 70±2 °C for 1.5 h. TEA was added to the final polymeric composite in order to create the ionic centers along the polymeric chains by neutralizing –COOH groups of BMPA. Finally, water was added at a very slow rate. THF was then removed under reduced pressure. Different weight percentages of CD@HAp nanohybrid, *viz.* 1, 2 and 3% were used in the fabrication process, which were coded as WHPU/CD@HAp1, WHPU/CD@HAp2 and WHPU/CD@HAp3, respectively. In order to get the nanocomposite films, these were further modified with 20 wt% of HE and 10 wt% of PAA as mentioned in Chapter 4 (Section 4.2.3.2.). Simultaneously, polymeric nanocomposites of HAp with WHPU, *viz.* WHPU/HAp1, WHPU/HAp2 and WHPU/HAp3 were also prepared by following the same method. Different properties of the nanocomposites were compared with a pristine system, which is equivalent to MWPU20 as described in Chapter 3. However, a general coding, i.e. MWPU has been adopted for MWPU20 in this chapter.

6.2.3.3. Cell proliferation assay

For cell proliferation and cytocompatibility studies, MG63 bone cells were seeded in 24-well cell culture plate at a density of 1×10^4 cells per well. Cells

were incubated at different concentrations of nanomaterials. The concentrations were selected as per the reports available.[14,15] Accordingly, concentration of 100 μg mL^{-1} was maintained for all the three variants of nanomaterial, *viz.* HAp, CD and CD@HAp. For CD@HAp, an additional concentration of 200 μg mL^{-1} was also prepared to assess toxicity at high concentration. Calculated amounts of the nanomaterials were mixed in culture medium (MEM) and were added to MG63 cell seeded wells. Culture wells without nanomaterial were kept as positive control. For cytocompatibility study of the nanocomposites, cells were cultured on all the five variants of the membranes, *viz.* MWPU, WHPU/HAp1, WHPU/HAp3, WHPU/CD@HAp1 and WHPU/CD@HAp3. For cell proliferation study, membranes (10 mm diameter) were pre-sterilized in laminar hood with 70% (v/v) ethanol for 3 h. Further, these membranes were washed with PBS (pH 7.4) and pre-conditioned in complete MEM. Cells were cultured on sterilized membranes at a density of 1×10^5 cells per membrane. Cell proliferation was determined on day 1, 3, 5 and 7 of culture using Alamar Blue reduction assay following manufacturers' protocol as described in Chapter 4 (Section 4.2.3.6.). Empty wells without cells supplemented with 10% Alamar Blue dye were used as the negative control.

6.2.3.4. Live/Dead assay

For Live/Dead assay, MG63 bone cells were seeded in 24-well cell culture plate at a density of 1×10^4 cells per well. Cells were incubated with calculated amount of nanomaterials (100 μg mL^{-1} for all the three nanomaterials, *viz.* CD, HAp and CD@HAp; an additional concentration of 200 μg mL^{-1} was used for CD@HAp) and analysed for their viability and adherence after 7 days of culture. Similarly, for nanocomposite membranes, Live/Dead assay was performed after 7 days of cell culture (1×10^5 cells per membrane) on different membranes. Live/Dead assay was performed according to the method described in Chapter 4 (Section 4.2.3.6.).

6.2.3.5. ALP assay

ALP activity of cultured MG63 cells in presence of nanomaterials (HAp, CD and CD@HAp) and nanocomposite films (MWPU, WHPU/HAp1, WHPU/HAp3, WHPU/CD@HAp1 and WHPU/CD@HAp3) was quantified by using ALP assay kit

(Abcam, USA). Briefly, MG63 cells cultured (for 7 days) with and without nanomaterials were harvested from tissue culture wells using 0.05% trypsin/EDTA and were washed with cold PBS. Similarly, MG63 cells cultured on the nanocomposite membranes were also harvested after 7 days of culture and washed with cold PBS. Harvested cells were re-suspended in 150 µL lysis buffer (0.2% (v/v)), Triton X-100 and 5 mM $MgCl_2$ provided in the kit. Subsequently, samples were centrifuged at 12,000 rpm and at 4 °C in a micro-centrifuge to remove any insoluble material. Supernatant was collected and transferred to clean tubes. Then the absorbance was measured at 405 nm using multimode reader.[16] ALP assay was performed according to manufacturer's instruction. Further, for easy depiction, the obtained values were normalized by reduced Alamar Blue reduction values and the results were plotted.

6.3. Results and discussion

6.3.1. Synthesis of CD@HAp

The present synthesis of CD@HAp nanohybrid employed one pot hydrothermal approach using bio-based precursors, *viz.* calcined egg shell as the calcium (Ca) source and aqueous extract of *C. esculenta* corm as the raw material for CD. **Scheme 6.1** demonstrates the synthesis of CD@HAp in a single pot process. The physico-chemical structure of CD played an important role in the synthesis of the nanohybrid. Careful characterization of CD showed that it has graphitic structure along with some disorderliness due to the presence of oxygen containing functionalities like hydroxyl, carboxylic, epoxy etc. as discussed in Chapter 4 (Section 4.3.1.).[17] These oxygen functional groups played the anchoring role in the synthesis of nano HAp structure with decorated CD over its surface. In the one pot process, CD was formed in the initial phase at the elevated temperature. These CDs interacted with Ca^{2+} through dative bond or undergo ion exchange with H^+ of carboxyl groups forming ionic interaction and thus provided the site for nucleation. On the other hand, the polyphenolic fraction of *C. esculenta* extract acted as a template for the formation of HAp nanostructure. They chelated Ca^{2+} ions through dative interaction forming [Ca–(polyphenolic)] complex. However, under hydrothermal condition, such interactions got weakened resulting in gradual release of Ca^{2+} ions. This helped in slowdown of nucleation and crystal growth process, which eventually facilitated integration of PO_4^{3-} and HO^- ions at the nucleation site. Thus, the current method was found

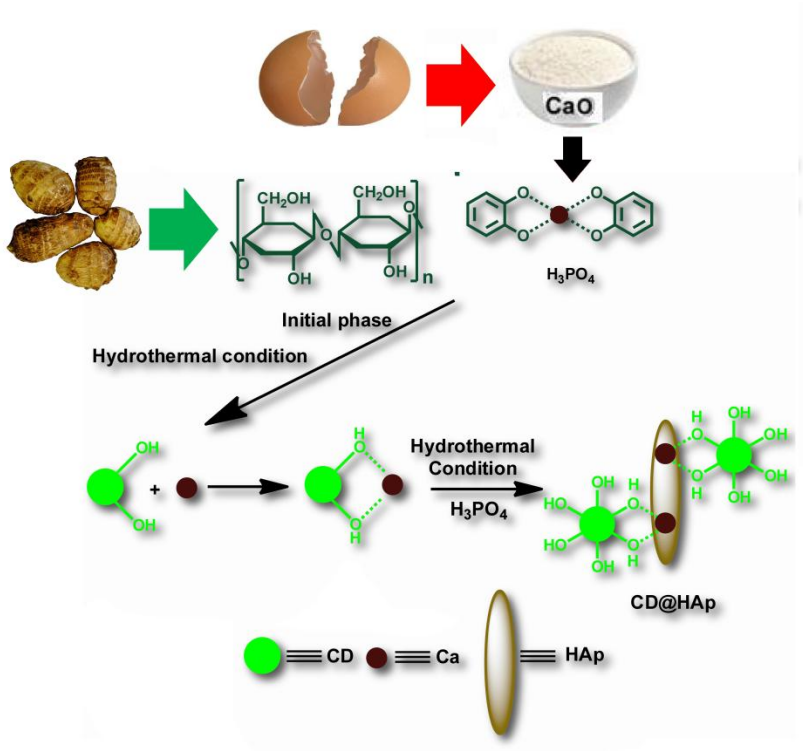

Scheme 6.1. Schematic presentation of hydrothermal synthesis of CD@HAp nanohybrid.

eloquent to obtain CD decorated HAp with controlled morphology. This CD@HAp nanohybrid was characterized with different spectroscopic and visual techniques and examined for osteogenic activities.

6.3.2. Characterization of CD@HAp

FTIR spectroscopic analysis confirmed the presence of characteristic chemical functionalities in the nanohybrid (**Figure 6.1a**). The sharp spike at 3572 cm^{-1} and medium sharp peak at 633 cm^{-1} are ascribed for the stretching and flexural modes of vibrations of lattice hydroxide entrapped within the closed pack structure of HAp, respectively.[18] The broad peak centered around 3450 cm^{-1} is due to absorbed H_2O molecule (in case of HAp) and -O-H groups of CD and absorbed H_2O molecule (in case of CD@HAp nanohybrid). Absorbance peak near 2920 cm^{-1}, which was found only in CD@HAp nanohybrid is assigned for -C–H stretching frequency. A peak with medium intensity was observed at frequency 1640 cm^{-1} for CD@HAp. However, the same was missing in HAp. This peak can be assigned to strong -C=O stretching frequency, which is present in CD. The characteristics PO_4^{3-} absorption peaks were observed at frequencies 1091, 1032, 962, 602, 564 and 572 cm^{-1}.[18] Thus, the FTIR characteristic

frequencies support the presence of both HAp and CD in the nanohybrid system. UV-visible spectra as depicted in **Figure 6.1b** divulge evidence in favor of the formation of the nanohybrid. For CD, absorption peak is generally observed in the 250-300 nm region, which represents typical aromatic-pi system.[19] For CD@HAp nanohybrid similar peak was observed at wavelength 268 nm. As, HAp does not exhibit any absorption in the UV-visible region, hence the above mentioned absorption shown by the nanohybrid confirmed the presence of CD along with HAp. Raman spectral analysis ensured the presence of graphitic carbon in the form of CD. The Raman spectrum of CD@HAp exhibited G band (characteristics of sp^2 hybridized carbon system) and D band (characteristics of disorder or defect) at wave numbers 1598 and 1345 cm^{-1}, respectively (**Figure 6.1c**). However, a slight red shift of D and G band was marked (compared to the band positions in CD), which can be attributed to the disorder caused in the graphitic structure of CD resulted from chemical and physical interactions with HAp nanocrystals. Higher value I_D/I_G ratio of CD@HAp (0.69) compared to only CD (0.62) further confirmed the fact. Typical Raman spectrum of the nanohybrid also displayed a peak at wavenumber 954 cm^{-1} that originates from the symmetric stretching mode vibration of PO_4^{3-}. XRD study was carried out for powder of egg shell, CaO and CD@HAp as depicted in **Figure 6.1d**. Egg shell mainly consists of $CaCO_3$ phase. The XRD pattern of egg shell displayed diffraction peaks at 2θ values of 23.2°, 29.6°, 36.2°, 39.4°, 43.2°, which are indexed as (012), (104), (110), (113) and (202) planes of $CaCO_3$, respectively. On heating at temperature 900 °C, these peaks disappeared and new peaks generated at 32.3°, 37.4°, 54.0°, 64.1° and 67.1°, which are assigned as (111), (200), (220), (311) and (222) planes of CaO phase, respectively. The XRD diffraction peaks for $CaCO_3$ and CaO phases are confirmed by comparing with the data obtained from ICDD-PDF-2 (data card number 85-1108 for $CaCO_3$ and data card number 48-1467 for CaO). Hence, XRD patterns confirmed the conversion of egg shell into CaO. On the other hand, a typical HAp diffraction pattern was observed for the synthesized nanohybrid. The major phase of HAp was confirmed by comparing with the data obtained from ICDD-PDF-2 (data card number 09-0432). The peaks at 31.6°, 32.0°, 33.5°, and 46.8° are assigned to the (211), (300), (202) and (222) reflection planes of HAp, respectively. In the XRD pattern, (002) plane of CD almost disappeared due to weak intensity and amorphous nature of carbon phase compared to highly intense HAp peaks. The XRD pattern is

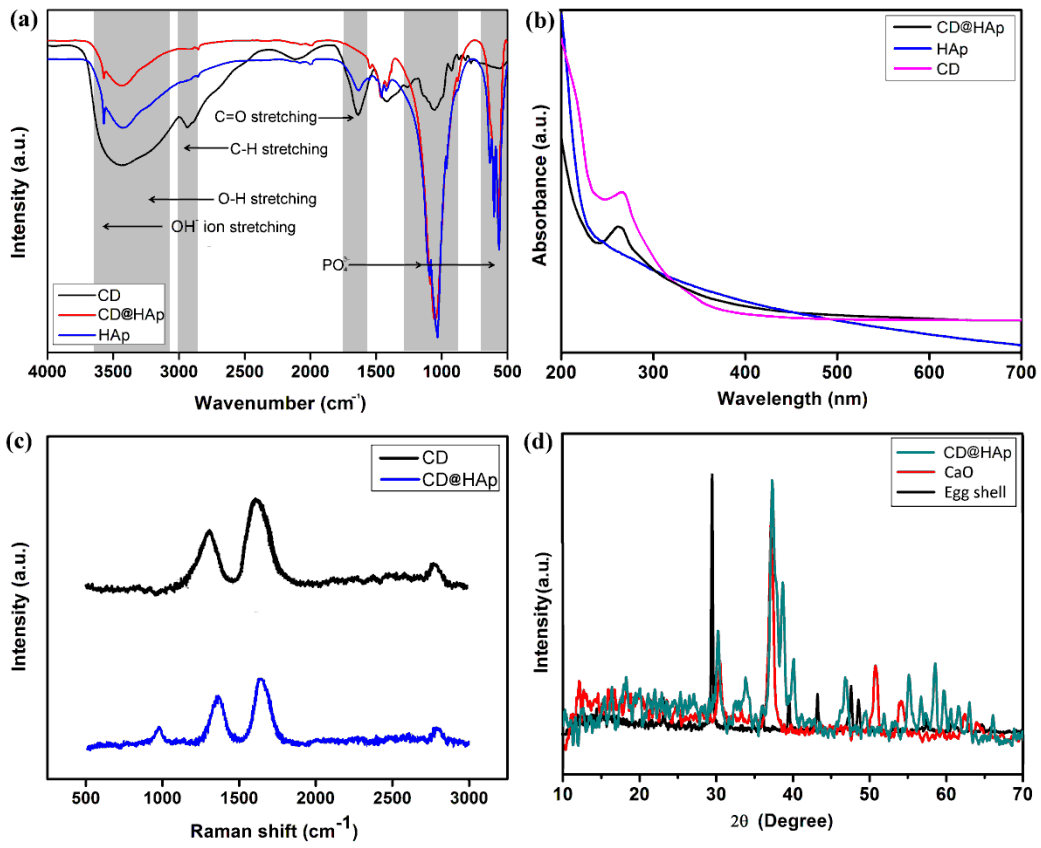

Figure 6.1. (a) FTIR spectra of CD, HAp and CD@HAp; **(b)** UV-visible spectra of CD, HAp and CD@HAp; **(c)** Raman spectra of CD and CD@HAp; **(d)** XRD patterns of egg shell ($CaCO_3$), CaO and CD@HAp.

quite helpful to acquire vital crystallographic evidences for the formation of nano HAp crystal. The crystallographic parameters for the prepared nanohybrid are obtained as a=b=9.425±0.003 Å and c=6.876±0.002 Å. These values coincide with those obtained from ICDD-PDF-2 data card for HAp (a=b=9.418 Å and c=6.884 Å). On the other hand, TEM micrographs furnished visual evidence confirming decoration of CD over the surface of HAp. The TEM images depicted in **Figure 6.2a** and **b** reveals needle shaped morphology with length of 50–80 nm and diameter of 20–30 nm. HRTEM image (**Figure 6.2c**) shows the decoration of CD over HAp nanoparticles. The distance between two conjugative planes in the lamellar structure of HAp was found as 0.284 nm, which is assigned as (211) plane of hexagonal HAp crystal. On the other hand, inter layer spacing of 0.211 nm can be indexed for the (001) plane of CD. IFFT of HRTEM of CD@HAp (inset of **Figure 6.2c**) further confirmed the assigned planes in the nanohybrid. The SAED pattern of CD@HAp nanohybrid displayed a clear

diffraction pattern with discrete spots indicating the formation of HAp nanocrystals (**Figure 6.2d**). The arrangement of the bright spots clearly indicates the presence of six fold symmetry. From the SAED pattern, (004), (310) and (211) planes of HAp can be assigned corresponding to *d* spacing of 0.172, 0.226 and 0.284 nm, respectively. The elemental analysis of the synthesized nanohybrid was further studied by SEM/EDX analysis. EDX spectrum as shown in **Figure 6.3** confirmed the presence of Ca, P, C and O in the nanohybrid. The ratio of Ca/P was found as 1.69, which is slightly greater than 1.67 found in natural bone.[20] But, it is very much close to the desired ratio and hence it can be expected that such nanohybrid system can stipulate extensive osteogenic activities. The elemental analysis further confirmed the presence of C and O in the system.

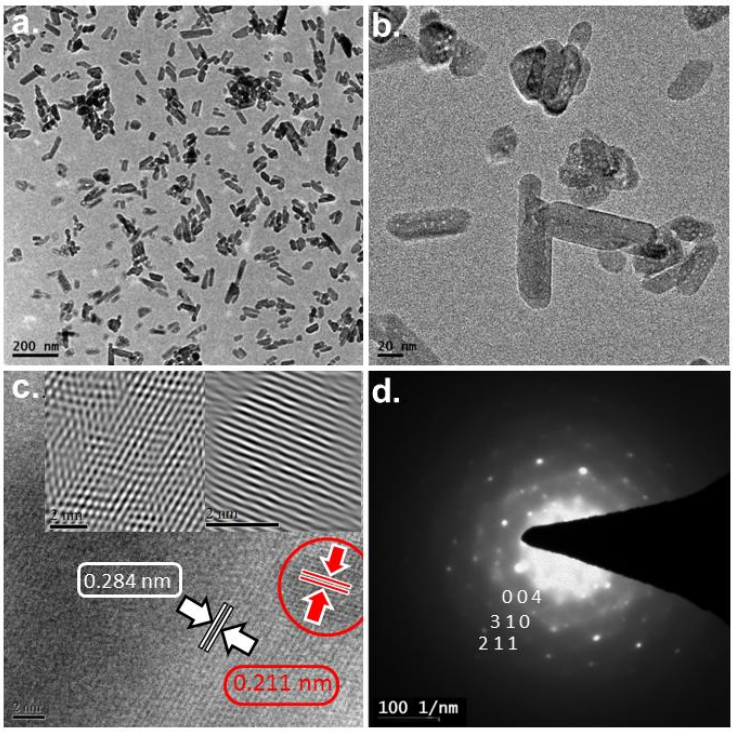

Figure 6.2. (a) and **(b)** TEM images of CD@HAp; **(c)** HRTEM image of CD@HAp (inset IFFT of HAp and CD phase in the nanohybrid); **(d)** SAED pattern of CD@HAp nanohybrid.

6.3.3. Fabrication of WHPU/CD@HAp nanocomposite

Although HAp possesses excellent osteogenic activity, it exhibits inferior mechanical properties, especially brittleness.[21] That is why apposite support is required for its functioning as bone implant material. Biocompatible polymers have been used for

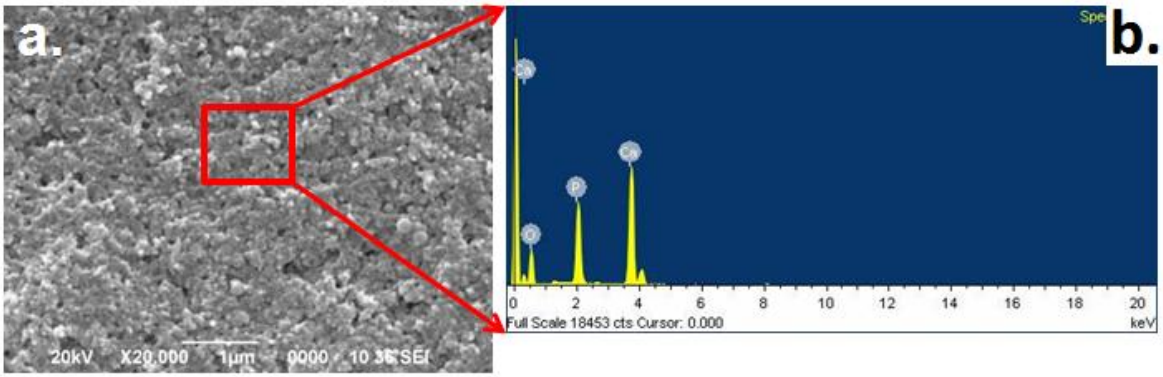

Figure 6.3. (a) Representative SEM image and **(b)** EDX spectrum of CD@HAp (Ca, P, O and C).

this purpose.[22] In the present study, we fabricated WHPU with the synthesized nanohybrid by following an *in situ* polymerization technique. In this context, we found CD decorated nano HAp more suitable than bare nano HAp. Generally, nano HAp lacks proper functionality, which is essential for *in situ* functionalization of any nanomaterial with a polymer matrix. However, decoration with CD resulted introduction of multi-functionality to HAp by means of various surface passivated groups. These multifunctional groups interacted with the polymer matrix either covalently or non-covalently. This leads to a uniform distribution of the nano-filler in the polymer matrix (**Scheme 6.2**). Such even sharing of HAp is very much essential for enhanced mechanical properties and biological activities of the polymeric nanocomposite films. TEM image (**Figure 6.4a**) confirmed a uniform distribution of

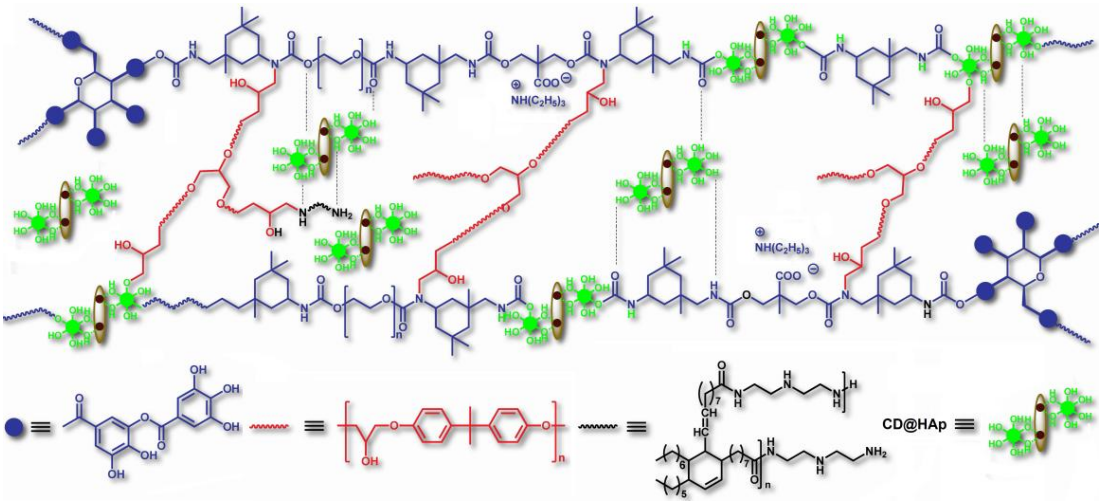

Scheme 6.2. Schematic presentation of *in situ* fabricated WHPU/CD@HAp nanocomposite.

the nanomaterial even at a high load (3%). FTIR spectra (**Figure 6.4b**) revealed a blue shift of peaks in the -C=O and -N–H region with increase amount of nano-filler loading in the polymer matrix. This shift of wavenumber is more pronounced in case of WHPU/CD@HAp nanocomposite compared to WHPU/HAp nanocomposite. This indicates existence of stronger secondary interactions in the former compared to the later.

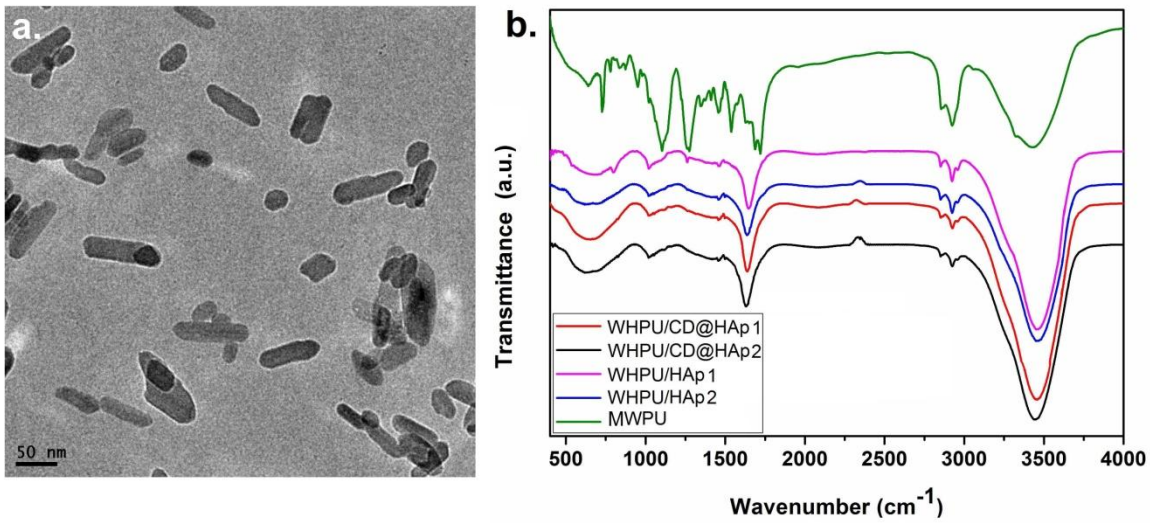

Figure 6.4. (a) TEM image of WHPU/CD@HAp3 and **(b)** FTIR spectra of MWPU, WHPU/HAp and WHPU/CD@HAp.

6.3.4. Mechanical properties

The mechanical properties of the nanocomposite were evaluated and results are presented in **Table 6.1**. Generally, bone tissue engineering requires material with high strength, toughness and flexibility.[23] Unfortunately, HAp is very brittle in nature, whereas pristine polymeric material alone cannot provide sufficient bioactivity and strength to design high load bearing prosthesis. But, the composite of both can provide material with high mechanical and biological properties through a synergic phenomenon.[24] The present study witnessed improvement of mechanical performance of the nanocomposites (for both WHPU/HAp and WHPU/CD@HAp). However, WHPU/CD@HAp nanocomposite showed much improved mechanical properties compared to WHPU/HAp. This can be ascribed for better dispersion of CD@HAp in the reaction medium compared to bare HAp. Surface decorated HAp with CD possesses varieties of oxygen functional groups, which interacted with the

Table 6.1. Mechanical properties of nanocomposites

Composition	Mechanical properties*					
	TS (MPa)	E@B (%)	Toughness§ (MPa)	SH† (kg)	IR‡ kJ m^{-1}	Gloss (60°)
MWPU#	17.0±0.5	220±2	28.74	9	8.25±0.1	95.2±0.3
WHPU/HAp1	18.4±0.6	205±3	30.87	>10	>8.30	95.1±0.2
WHPU/HAp2	20.8±0.5	192±3	32.41	>10	>8.30	94.6±0.4
WHPU/HAp3	21.3±0.3	175±3	29.38	>10	>8.30	92.8±0.5
WHPU/CD@HAp1	20.4±0.3	221±2	38.26	>10	>8.30	94.3±0.3
WHPU/CD@HAp2	23.3±0.4	212±4	40.23	>10	>8.30	93.8±0.2
WHPU/CD@HAp3	28.4±0.3	198±2	41.30	>10	>8.30	92.4±0.4

**Mechanical properties: TS=Tensile strength, E@B=Elongation at break, SH=Scratch hardness, IR=Impact resistance; §Obtained by calculating area under stress-strain curve; †Limit of scratch hardness tester was 10 kg (maximum); ‡Limit of impact tester is 8.30 kJ m^{-1} for film of thickness 1mm (maximum). #Data presented from Chapter 3 for comparison.*

polymer matrix either covalently or through secondary interactions as discussed in the previous section. This provided a uniform distribution of the nanomaterial over the polymer matrix without any agglomeration. Further, functional groups of CD acted as additional reaction sites for cross-linking reactions to occur. This increased the cross-linking density within the macromolecular structure. All these factors contributed significantly towards enhanced mechanical properties of WHPU/CD@HAp nanocomposite. On the other hand, fabrication of WHPU with HAp and CD@HAp lead to diminution of elongation at break values. However, extent of reduction in elongation was found more for WHPU/HAp nanocomposite compared to WHPU/CD@HAp. Better elongation at break values of WHPU/CD@HAp nanocomposite can be attributed to the layered structure of CD, which imparts good flexibility to the polymer matrix.[25] All the nanocomposite films possessed bending value of 2 mm. Such good flexibility is essential for any bone implant material. The enhancement of mechanical properties was found to be nano-material dose dependent for both WHPU/CD@HAp and WHPU/HAp nanocomposites. Thus, overall performance of WHPU/CD@HAp was found better than WHPU/HAp, which indicates aptness of the former compared to the later for high load bearing biomedical utility.

6.3.5. Thermal properties

The thermal degradation of egg shell was carried out, which displayed a weight loss of ~45% at 900 °C (**Figure 6.5a**). The substantial weight loss occurred at temperature 830 °C. There after an almost steady phase was obtained without further reduction in weight. Such typical TG curve gives the hint of conversion of $CaCO_3$ phase into CaO phase.[26,27] On the other hand, thermal degradation analysis of the nanohybrid was conducted in order to study the degradation pattern. An initial degradation above 100 °C was witnessed for both HAp and CD@HAp systems (**Figure 6.5b**). This happened by the evaporation of moisture absorbed by the nanomaterial as well as release of trapped water molecules present within HAp crystal. As such HAp is thermally very stable. It is well reflected by the TG thermogram of HAp. From 25 °C to 800 °C, only 5.8% weight loss was recorded. However, CD is sensitive towards heat. Hence, a substantial weight loss was perceived (12.7 wt% from 25–800 °C) in case of CD@HAp nanohybrid. Similar to HAp, an initial weight loss was witnessed for CD@HAp nanohybrid above 100 °C. A second degradation was observed from 265 °C, which was mainly due to the degradation of carbon phase of the nanohybrid system. On the other hand, the thermal degradation pattern of the nanocomposite films revealed a dose dependent improvement of thermal stability (**Figure 6.6**). Increasing amount of nanomaterial loading imparted more cross-linking density and secondary interactions to the polymer matrix as described in Section 6.3.4. This leads to improved thermo-stability of the polymeric nanocomposite system.

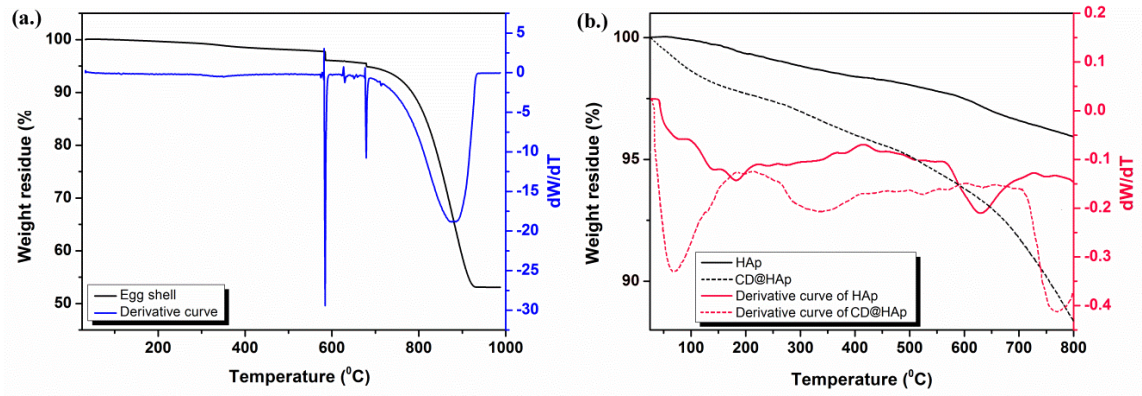

Figure 6.5. (a) TG and corresponding derivative curves of egg shell and **(b)** TG and corresponding derivative curves and HAp and CD@HAp.

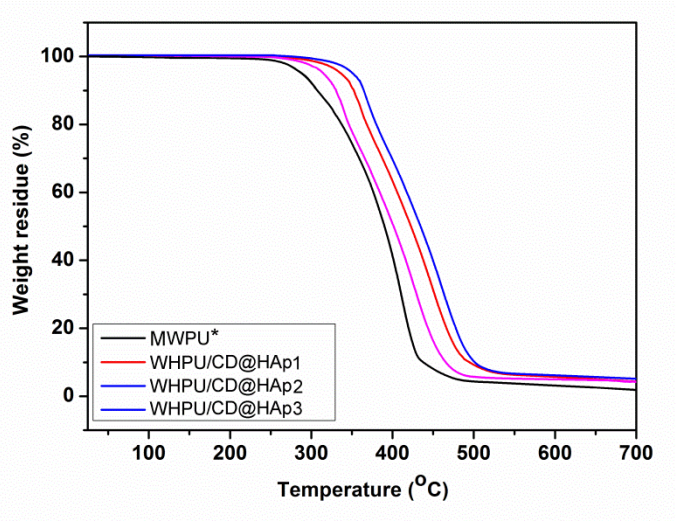

Figure 6.6. TG thermograms of WHPU/CD@HAp nanocomposite.*Data reproduced from Chapter 3 for comparison.

6.3.6. Biological properties

6.3.6.1. Cell proliferation and cytocompatibility

Cell proliferation and cytocompatibility studies were performed to determine the effect of nanomaterials on viability and proliferation of MG63 cells. Alamar Blue assay quantified cellular viability and proliferation over time in the presence of various nanomaterials. Obtained results indicate normal cellular proliferation within the wells when cultured in the presence of nanomaterials without any signs of toxicity or inhibition. The obtained Alamar reduction values in the presence of nanomaterials were comparable to the positive control wells ($p>0.05$) (**Figure 6.7a**). High reduction in Alamar Blue over time, which relates number of proliferating cells and enhanced cellular metabolism suggests cytocompatibility of the nanomaterials.[28,29] After 7 days of culture, MG63 cells showed the following trend: ~2.53 fold enhancement in presence of CD@HAp (100 µg mL^{-1})>~2.52 fold with positive control>~2.48 fold with CD@HAp nanohybrid (200 µg mL^{-1})>~2.44 fold with CD (100 mg mL^{-1}) and ~2.43 fold with HAp (100 µg mL^{-1}) compared to day 1 of culture. No significant difference was observed between the groups ($p>0.05$) on day 7 suggesting that there was no inhibitory effect of the added nanomaterials on cell viability and proliferation. From this preliminary cell proliferation and cytocompatibility results it is assumed that CD@HAp nanohybrid can serve as a potent candidate for bone regeneration. Further, *in vitro* cell proliferation study was performed on the nanocomposite membranes, *viz.*

MWPU, WHPU/HAp1, WHPU/HAp3, WHPU/CD@HAp1 and WHPU/CD@HAp3 using MG63 cells. Equal number of cells was seeded on these membranes and cell proliferation was quantified over time. On day 7 of culture, cell proliferation rate revealed the following trend: ~2.52 fold enhancement on WHPU/CD@HAp3>~2.49 fold on WHPU/CD@HAp1>~2.39 fold on WHPU/HAp3 >~2.11 fold on WHPU/HAp1 and >~1.91 fold on MWPU compared to day 1 of culture (**Figure 6.7b**). On day 7, all the membranes exhibited significant differences in cell proliferation when compared with the control. There exists a highly significant difference in cell proliferation on MWPU with WHPU/CD@HAp1 and WHPU/CD@HAp3 ($p<0.01$). A concentration dependent effect of nanomaterial on cell proliferation of WHPU/HAp1 and WHPU/HAp3 ($p<0.01$) was also witnessed. Membranes having CD@HAp aided better cell proliferation as depicted from the graph and there was a highly significant difference of cell proliferation on WHPU/CD@HAp1 and WHPU/CD@HAp3 when compared with WHPU/HAp1 ($p<0.01$). This shows the effect of addition of CD on cell proliferation. Alamar Blue reduction value suggests that the nanocomposite membranes are cytocompatible for biological applications especially for bone regeneration. HAp, a major component of human bone has been extensively used in bone regeneration studies and it is a well-established biomaterial in tissue engineering and regenerative medicine.[30,31] Similarly, CD is also reported as a highly

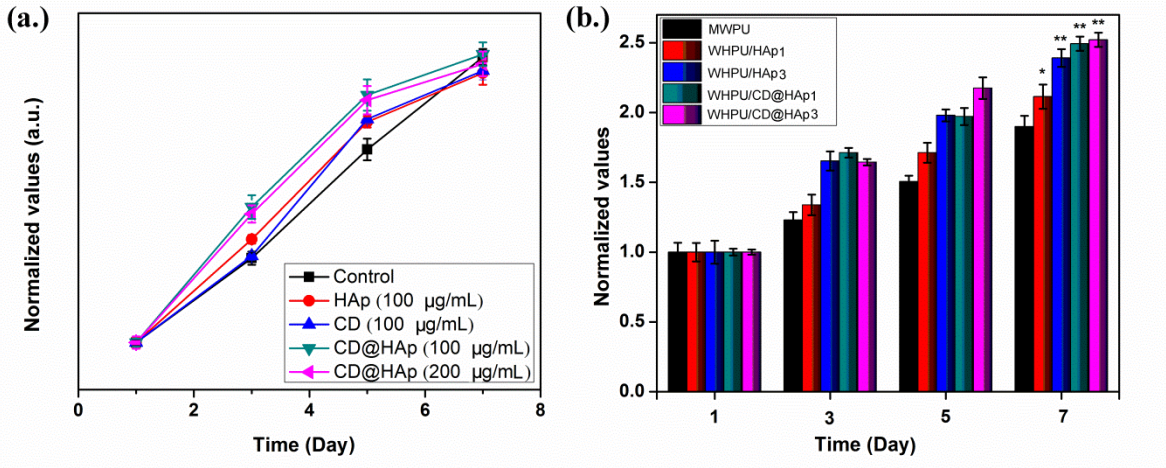

Figure 6.7. (a) Alamar Blue cell proliferation graph showing MG63 cell proliferation with different nanomaterials; **(b)** Alamar Blue cell proliferation graph showing MG63 cell proliferation on different nanocomposite membranes. Data represented as the average±standard deviation. (* $p < 0.05$, ** $p < 0.01$).

cytocompatible material and extensively used in making bio-composites having superior physico-chemical and biological properties. Recent reports have shown that rough surfaces can accelerate osteoblast cell attachment and proliferation potential.[12,32,33] Higher rate of cell proliferation on WHPU/CD@HAp compared to WHPU/HAp is attributed to the surface roughness provided by CD, which were decorated over HAp surface. Additionally, CD@HAp has provided additional advantage of uniform distribution over the polymer matrix, which facilities enhanced and uniform tissue regeneration capability of WHPU/CD@HAp nanocomposite. Thus, these membranes could further be utilized as prospective material for accelerated tissue regeneration applications.

6.3.6.2. Live/Dead assay

Live/Dead assay showed attachment and viability of MG63 cells when cultured in the presence of nanomaterials and nanocomposite films. Cells exhibited native spindle morphology and were uniformly distributed within the culture wells and on the nanocomposite membranes (**Figure 6.8** and **6.9**). Live/Dead assay results are

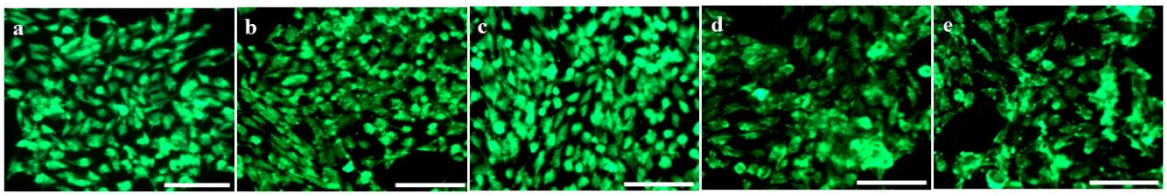

Figure 6.8. Fluorescent microscopic images showing MG63 cells growing in tissue culture wells after 7 days of culture: **(a)** control (without nanomaterial), **(b)** HAp (100 μg mL^{-1}), **(c)** CD (100 μg mL^{-1}), **(d)** CD@HAp (100 μg mL^{-1}) and **(e)** CD@HAp (200 μg mL^{-1}). Scale bar represents 100 μm.

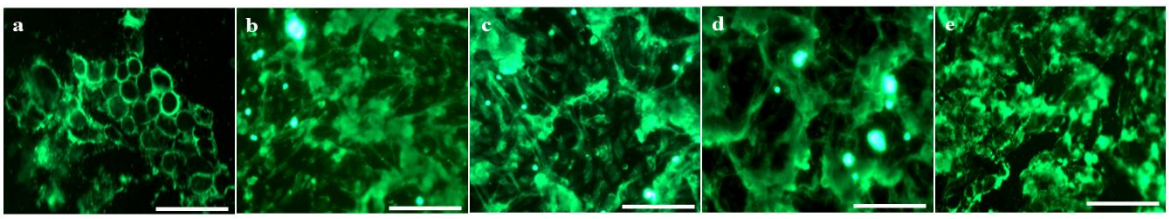

Figure 6.9. Fluorescent microscopic images showing MG63 cells growing on membranes after 7 days of culture: **(a)** MWPU, **(b)** WHPU/HAp1, **(c)** WHPU/HAp3, **(d)** WHPU/CD@HAp1 and **(e)** WHPU3/CD@HAp. Scale bar represents 100 μm.

consistent with Alamar Blue cell proliferation data, which suggest cytocompatibility of CD@HAp nanohybrid and composite membranes. As evident from the fluorescence microscopic images, proliferating cells formed close clusters within the wells. On the nanocomposite membranes, cells were more spread and possessed spindle like native morphology (**Figure 6.9**). Cells were relatively spherical on control (MWPU) membrane. Cell clusters formed on the membranes may help in better cell to cell interactions and extracellular matrix (ECM) deposition. Enhanced ECM deposition overtime is the most desired attributes in tissue regeneration, as greater ECM would lead to the formation of mature functional tissues similar to native one.[34]

6.3.6.3. ALP assay

ALP activity is a hallmark of osteoblast cells and is expressed in cell differentiation phase. It is a quantitative marker for osteogenesis.[28] *In vitro* ALP activity of cultured MG63 cells was measured by the conversion of *p*-nitro phenyl phosphate to *p*-nitro phenol. Further, for meaningful data representation, ALP activity was normalized with the Alamar Blue reduction values. Results showed that CD@HAp exhibited high ALP activity, which was comparable to HAp (**Figure 6.10a**). As evident from the graph, significantly higher ALP activity was noted within the wells incubated with nanomaterials in comparison to the control ($p<0.05$). On the other hand, ALP activity on different nanocomposite membranes revealed the following trend: ~22.38 U L^{-1} on WHPU/CD@HAp3>~22.18 U L^{-1} on WHPU/CD@HAp1>~21.95 U L^{-1} on WHPU/HAp3 >~21.76 U L^{-1} on WHPU/HAp1 and >~19.4 U L^{-1} on control (MWPU) (**Figure 6.10b**). From the trend it is clear that nanocomposite membranes possessed significantly higher ALP activity compared to the control (MWPU) ($p<0.01$). HAp being osteoconductive and biocompatible material helped in maintaining differentiated phase of osteoblast cells with enhanced bone like ECM formation.[35] It also acted as the nucleation sites helping mineral deposition by cells leading to increased bone matrix production.[35,36] Recent studies have shown that carbon-based nanomaterials (e.g. graphene, graphene oxide, graphite, carbon nano tube etc.) with or without HAp to be supportive for osteogenic cell proliferation and differentiation processes.[9-12] They help in oriented nucleation and growth of HAp for osteogenic differentiation. Presence of graphitic structure further promotes adherence of human osteoblast cells.[37] Being a carbon family member with graphitic sp^2 carbon structure,

CD also acted in a similar fashion, which results enhanced ALP activity of WHPU/CD@HAp nanocomposite. It is a known fact that the presence of acidic groups on the surface of an implant enhances phagocytosis of the material by macrophages in soft tissue, while the basic groups on carbon surface are advantageous for regenerative processes of bone tissues.[38] CD having various surface functional groups is thus expected to help in the bone regeneration process. Further, decorated CD can provide kind of roughness over HAp surface, which also contributed towards enhanced osteogenic activity of WHPU/CD@HAp nanocomposite. Profound ALP activity within the wells containing CD@HAp and WHPU/CD@HAp films thus suggests potentiality of the nanocomposite system for bone related applications.

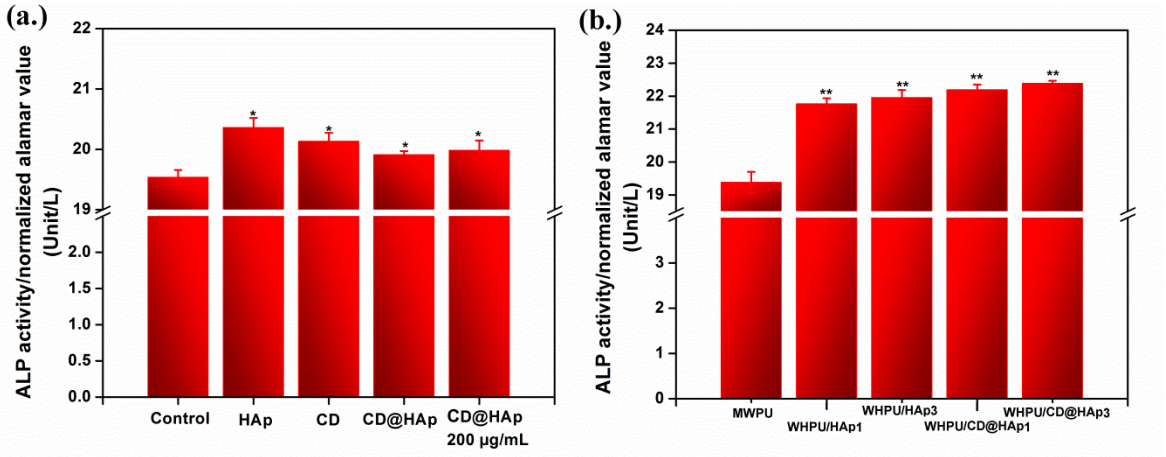

Figure 6.10. Graph showing ALP activity of MG63 cells after 7 days: **(a)** with different nanomaterials and **(b)** on different nanocomposite membranes. Data represented as the average±standard deviation. (* $p < 0.05$, ** $p < 0.01$).

6.4. Conclusion

Thus, the present study demonstrated a facile one pot synthesis of carbon dot decorated hydroxyapatite nanohybrid using egg shell as a waste source and corms of *Colocasia esculenta* as a bio-based source. Carbon dot nanoparticles were found to be decorated over the surface of hydroxyapatite nano needles. Cytocompatibility assessment of the nanohybrid showed that there is no adverse effect of incorporation of carbon dot with hydroxyapatite even at a high concentration on MG63 cells. Rather, enhanced cell proliferation was observed after decoration with carbon dot. Moreover, the nanohybrid demonstrated profound cell adherence and alkaline phosphatase activity against MG63 cell line. This nanohybrid was successfully used to

fabricate tannic acid based waterborne hyperbranched polyurethane system by following an *in situ* technique. Evaluation of properties showed excellent gain in mechanical performance and biological activity. The results endorse the role of decorated graphitic carbon nanoparticle/hydroxyapatite hybrid system to achieve a high load bearing, biologically active polymeric nanocomposite, which could be used as bone replacement material. Further, use of renewable resource based materials and benign solvent system justifies the sustainability of the developed system.

References

(1) Chapekar, M.S. Tissue engineering: Challenges and opportunities, *J. Biomed. Mater. Res., Part A* **53**, 617--620, 2000.

(2) Armentano, I., et al. Biodegradable polymer matrix nanocomposites for tissue engineering: A review, *Polym. Degrad. Stab.* **95**, 2126--2146, 2010.

(3) Sahithi, K., et al. Polymeric composites containing carbon nanotubes for bone tissue engineering, *Int. J. Biol. Macromol.* **46**, 281--283, 2010.

(4) Suchanek, W., & Yoshimura, M. Processing and properties of hydroxyapatite-based biomaterials for use as hard tissue replacement implants, *J. Mater. Res.* **13**, 94--117, 1998.

(5) Sadat-Shojai, M., et al. Synthesis methods for nano-sized hydroxyapatite with diverse structures, *Acta Biomater.* **9**, 7591--7621, 2013.

(6) Zhou, H., & Lee, J. Nanoscale hydroxyapatite particles for bone tissue engineering, *Acta Biomater.* **7**, 2769--2781, 2011.

(7) Nejati, E., et al. Synthesis and characterization of nano-hydroxyapatite rods/poly (l-lactide acid) composite scaffolds for bone tissue engineering, *Composites, Part A* **39**, 1589--1596, 2008.

(8) Tanigawa, H., et al. Electrochemical corrosion and bioactivity of titanium–hydroxyapatite composites prepared by spark plasma sintering, *Corros. Sci.* **70**, 212--220, 2013.

(9) Baradaran, S., et al. Mechanical properties and biomedical applications of a nanotube hydroxyapatite-reduced graphene oxide composite, *Carbon* **69**, 32--45, 2014.

(10) Fan, Z., et al. Mechanical properties and biomedical applications of a nanotube hydroxyapatite-reduced graphene oxide composite, *Carbon* **66**, 407--416, 2014.

(11) Lavanya, N., et al. A new strategy for simultaneous determination of 4-aminophenol, uric acid and nitrite based on a graphene/hydroxyapatite composite modified glassy carbon electrode, *RSC Adv.* **5**, 52703--52709, 2015.

(12) Zhang, L., et al. A tough graphene nanosheet/hydroxyapatite composite with improved in vitro biocompatibility, *Carbon* **61**, 105--115, 2013.

(13) Jazie, A., et al. Egg shell as eco-friendly catalyst for transesterification of rapeseed oil: Optimization for biodiesel production, *Int. J. Green Econ.* **2**, 27--32, 2013.

(14) Li, M., et al. In situ synthesis and biocompatibility of nano hydroxyapatite on pristine and chitosan functionalized graphene oxide, *J. Mater. Chem. B* **1**, 475--484, 2013.

(15) Liu, H., et al. Simultaneous reduction and surface functionalization of graphene oxide for hydroxyapatite mineralization, *J. Phys. Chem. C* **116**, 3334--3341, 2012.

(16) Stratford, E.W., et al. The tankyrase-specific inhibitor JW74 affects cell cycle progression and induces apoptosis and differentiation in osteosarcoma cell lines, *Cancer Med.* **3**, 36--46, 2014.

(17) De, B., & Karak, N. A green and facile approach for the synthesis of water soluble fluorescent carbon dots from banana juice, *RSC Adv.* **3**, 8286--8290, 2013.

(18) Chen, F., et al. Preparation and characterization of nano-sized hydroxyapatite particles and hydroxyapatite/chitosan nano-composite for use in biomedical materials, *Mater. Lett.* **57**, 858--861, 2002.

(19) Li, H., et al. One-step ultrasonic synthesis of water-soluble carbon nanoparticles with excellent photoluminescent properties, *Carbon* **49**, 605--609, 2011.

(20) Tas, A.C., et al. An investigation of the chemical synthesis and high-temperature sintering behaviour of calcium hydroxyapatite (HA) and tricalcium phosphate (TCP) bioceramics, *J. Mater. Sci.: Mater. Med.* **8**, 91--96, 1997.

(21) Yoshinari, M., et al. Properties of hydroxyapatite-coated Ti-6Al-4V alloy produced by the ion-plating method, *Bull. Tokyo. Dent. Coll.* **32**, 147--156, 1991.

(22) Chang, M.C., & Tanaka, J. FT-IR study for hydroxyapatite/collagen nanocomposite cross-linked by glutaraldehyde, *Biomaterials* **23**, 4811--4818, 2002.

(23) Hutmacher, D.W. Scaffolds in tissue engineering bone and cartilage, *Biomaterials* **21**, 2529--2543, 2000.

(24) Wei, G., & Ma, P.X. Structure and properties of nano-hydroxyapatite/polymer composite scaffolds for bone tissue engineering, *Biomaterials* **25**, 4749--4757, 2004.

(25) De, B., et al. Transparent luminescent hyperbranched epoxy/carbon oxide dot nanocomposites with outstanding toughness and ductility, *ACS Appl. Mater. Interfaces* **5**, 10027--10034, 2013.

(26) Khemthong, P., et al. Industrial eggshell wastes as the heterogeneous catalysts for microwave-assisted biodiesel production, *Catal. Today* **190**, 112--116, 2012.

(27) Niju, S., et al. Modification of egg shell and its application in biodiesel production, *J. Saudi Chem. Soc.* **18**, 702--706, 2014.

(28) Mandal, B.B., et al. High-strength silk protein scaffolds for bone repair, *Proc. Natl. Acad. Sci.* **109**, 7699--7704, 2012.

(29) Mandal B.B., & Kundu, S.C. Cell proliferation and migration in silk fibroin 3D scaffolds, *Biomaterials* **30**, 2956--2965, 2009.

(30) Itokazu M., & Matsunaga, T. Arthroscopic restoration of depressed tibial plateau fractures using bone and hydroxyapatite grafts, *Arthroscopy* **9**, 103--108, 1993.

(31) Nie, H., et al. BMP-2 plasmid loaded PLGA/HAp composite scaffolds for treatment of bone defects in nude mice, *Biomaterials* **30**, 892--901, 2009.

(32) Bhadang, K.A., et al. Biological responses of human osteoblasts and osteoclasts to flame-sprayed coatings of hydroxyapatite and fluorapatite blends, *Acta Biomater.* **6**, 1575--1583, 2010.

(33) Ribeiro, N., et al. Influence of crystallite size of nanophased hydroxyapatite on fibronectin and osteonectin adsorption and on MC3T3-E1 osteoblast adhesion and morphology, *J. Colloid. Interface Sci.* **351**, 398--406, 2010.

(34) Allori, A.C. Biological basis of bone formation, remodeling, and repair-part II: Extracellular matrix, *Tissue Eng., Part B* **14**, 275--283, 2008.

(35) Bhumiratana, S., et al. Nucleation and growth of mineralized bone matrix on silk-hydroxyapatite composite scaffolds, *Biomaterials* **32**, 2812--2820, 2011.

(36) Norman, M.E., et al. An in-vitro evaluation of coralline porous hydroxyapatite as a scaffold for osteoblast growth, *Clin. Mater.* **17**, 85--91, 1994.

(37) Kalbacova, M., et al. Graphene substrates promote adherence of human osteoblasts and mesenchymal stromal cells, *Carbon* **48**, 4323--4329, 2010.

(38) Blazewicz, M. Carbon materials in the treatment of soft and hard tissue injuries, *Eur. Cells Mater.* **2**, 21--29, 2001.